Phase characters of optical dark solitons with third-order dispersion and delayed nonlinear response

Yan-Hong Qin,[1] Xiaoman Zhang,[1] Liming Ling,[1,*] and Li-Chen Zhao[2,3,4,†]
[1]*School of Mathematics, South China University of Technology, Guangzhou 510640, China*
[2]*School of Physics, Northwest University, Xi'an 710127, China*
[3]*Shaanxi Key Laboratory for Theoretical Physics Frontiers, Xi'an 710127, China*
[4]*Peng Huanwu Center for Fundamental Theory, Xi'an 710127, China*

(Received 1 April 2022; accepted 4 August 2022; published 25 August 2022)

Dark soliton is usually seen as one of the simplest topological solitons, due to phase shift across its intensity dip. We investigate phase characters of single-valley dark soliton (SVDS) and double-valley dark soliton (DVDS) in a single-mode optical fiber with third-order dispersion and delayed nonlinear response. Notably, two different phase shifts can produce an SVDS with the same velocity under some conditions, which is not admitted for a dark soliton with only the second-order dispersion and self-phase modulation, whose phase shift and velocity is a one-to-one match. This phase property of SVDS can be used to explain the generation of previously reported DVDS in Hirota equation and make DVDSs show two types of phase profiles. Moreover, the different topological vector potentials underlying the distinct phase profiles have been uncovered. We further explore the collision properties of the DVDSs by analyzing their topological phases. Strikingly, the inelastic collision can lead to the conversion between the two types of phase profiles for DVDS. The results reveal that inelastic or elastic collision can be judged by analyzing virtual topological magnetic fields.

DOI: 10.1103/PhysRevE.106.024213

I. INTRODUCTION

Nonlinear optical fibers are known to be the most convenient quasi-one-dimensional system to investigate dynamical properties of solitons, owing to the simplicity and precise control on the experimental parameters [1–5]. In the picosecond regime, the propagation of optical pulses is modeled by the one-dimensional nonlinear Schrödinger equation (NLSE) [6,7], which accounts for the second-order dispersion and self-phase modulation. This generic model with self-defocusing (self-focusing) nonlinearity admits dark (bright) soliton [6,7]. In contrast to the bright soliton, dark soliton has a nontrivial distribution of their phase, so there exists a finite phase shift across the intensity dip [3,4]. Because of this, dark soliton is usually seen as one of the simplest topological solitons [8–10]. A phase shift is always necessary to create a dark soliton in experiments [3,4], which is absent for usual bright solitons. This has been confirmed in many dark soliton experiments [2–4]. Generally, an abrupt π phase shift produces a stationary dark soliton [2–4]. While a continuous changing phase creates a moving dark soliton, the dependence of the momentum on the velocity determines its stability [11,12]. Recently, the intriguing topological phases of the SVDS in scalar NLSE and multivalley dark soliton in vector NLSE have been revealed [13,14], via extending the complex coordinate space to explore the intensity zeros of dark solitons. The phase variations of dark solitons are usually velocity-dependent. Specifically, there is a one-to-one match between the phase shift and velocity of dark solitons in NLSE [3,4,13,14].

For ultrashort pulses (in the subpicosecond or femtosecond regime), the higher-order effects such as higher-order dispersion and delayed nonlinear response can no longer be ignored [15,16]. In this case, the evolution of optical solitons follows from the higher-order NLSE rather than the standard NLSE, such as the Hirota equation (HE) and Sasa-Satsuma equation [15–22]. Remarkably, a recent study has demonstrated that in the single-mode HE, a single dark soliton can admit two kinds of intensity profiles [23]. One is the well-known dark soliton which generally has a single valley (denoted as SVDS). The other is a dark soliton with double valleys (denoted as DVDS). The DVDS cannot exist in scalar NLSE, and their formation mechanism in HE is still not explained well. On the other hand, the phase properties of these dark solitons with high-order effects have not been studied systematically. Noting that the DVDS is composed of two parallel SVDSs [20,23,24], we expect that the relations between phase shift and velocity of an SVDS could be helpful in understanding the formation mechanism of DVDSs.

In this study, we focus on the phase properties of dark solitons in a single-mode optical fiber with the third-order dispersion and delayed nonlinear response, with the aid of exact dark solitons solution of scalar defocusing HE. Interestingly, there are two types of correspondence relations between the velocity and phase shift of an SVDS under some conditions. For type I, there is a one-to-one match between the phase shift and velocity, similar to the ones in NLSE. For type II, an SVDS at the same velocity possesses two different phase profiles; that is why the DVDS can be formed in scalar HE. The phase profile of a DVDS can be U-shaped or double-step

*linglm@scut.edu.cn
†zhaolichen3@nwu.edu.cn

type. We present the existence diagrams for the two types of correspondence relations with varying the background wave number or the higher-order nonlinearity. Meanwhile, the different topological vector potentials underlying the distinct phase shifts have been revealed. Furthermore, we discuss solitons' collision containing the DVDSs from a phase standpoint, via combining the topological vector theory with the developed asymptotic analysis technique. Strikingly, the type of phase distribution of a DVDS can be changed after the inelastic collision, due to the variations of virtual topological magnetic fields. The inelastic collision must result in changes in topological magnetic fields in the complex space. For the elastic collision, both the intensity and phase profiles remain unchanged. These phase properties provide an alternative approach to understanding dark solitons' physical mechanism and collision properties.

Our paper is organized as follows. In Sec. II, we present the physical model and study phase characters of an SVDS. The existence diagrams for the two types of correspondence relations between the velocity and phase shift are presented. In Sec. III, two types of phase distributions for a DVDS with the same velocity have been studied in detail. In Sec. IV, we discuss the collision properties of DVDSs based on the topological vector potential theory and the asymptotic analysis technique. Finally, the summary is given in Sec. V.

II. PHYSICAL MODEL AND PHASE CHARACTERS OF SINGLE-VALLEY DARK SOLITON

The single mode optical fibers with the third-order dispersion and delayed nonlinear response can be governed by the well-known HE [17–19]. In dimensionless form it is given by

$$i\frac{\partial q}{\partial t}+\frac{1}{2}\frac{\partial^2 q}{\partial x^2}+\sigma|q|^2 q-i\beta\left(\frac{\partial^3 q}{\partial x^3}+6\sigma|q|^2\frac{\partial q}{\partial x}\right)=0, \quad (1)$$

where t, x are time evolution and spatial distribution coordinates, and $q(x,t)$ is the envelope of the wave field. However, in the context of optical fibers, the roles of t and x are reversed. This model can describe the propagations of ultrashort light pulses, such as subpicosecond or femtosecond pulses. The last two terms in Eq. (1) that enter with a real coefficient β are responsible for the third-order dispersion and delayed nonlinear response, respectively. Based on the integrability of HE, many kinds of exact localized wave solutions have been obtained by various methods. There are dark solitons in defocusing case ($\sigma=-1$) [20,23–26], and bright solitons, rogue waves, rational solitons and breathers in focusing case ($\sigma=1$) [21,22,27–32].

In this study, we will investigate the phase characters of SVDS and DVDS in defocusing case, based on the exact n-dark solitons solution [see Eq. (A5)] of Eq. (1). The detailed derivation processes have been given in Appendix A, by applying n-fold Darboux transformation (DT) on plane wave background $q^{[0]}=ce^{i\theta}$ with $\theta=ax-[\beta(a^2+6c^2)a+1/2a^2+c^2]t$ [33]. Here, c and a are the amplitude and wave number of the background, respectively. Since the units of Eq. (1) are dimensionless, the background velocity equals the value of wave number, based on the quantum mechanics theory [34]. In our calculations, we introduce the spectral parameters with the form $\lambda_i=c\cos z_i-\frac{a}{2}$ [$z_i\in(0,\pi)$, $i=1,\ldots,n$] to simplify soliton solutions.

TABLE I. The velocity ranges of SVDS. Here, the expressions $v_{ds}|_{z_1=\pi}=3\beta(a^2+2ac+2c^2)+c$, $v_{ds}|_{z_1=0}=3\beta(a^2-2ac+2c^2)-c$, $v_{ds}|_{z_1=z_e}=(3a^2+2c^2)\beta-\frac{(1+6a\beta)^2}{16\beta}$, and $z_e=\arccos(\frac{\rho}{2})$ with $\rho=(6a\beta+1)/(4c\beta)$.

β	a	v_{ds}
$\beta>0$	$a<-\frac{8c\beta+1}{6\beta}$	$v_{ds}\|_{z_1=\pi}\leqslant v_{ds}\leqslant v_{ds}\|_{z_1=0}$
	$a>\frac{8c\beta-1}{6\beta}$	$v_{ds}\|_{z_1=0}\leqslant v_{ds}\leqslant v_{ds}\|_{z_1=\pi}$
	$-\frac{1}{6\beta}\leqslant a<\frac{8c\beta-1}{6\beta}$	$v_{ds}\|_{z_1=z_e}\leqslant v_{ds}\leqslant v_{ds}\|_{z_1=\pi}$
	$-\frac{8c\beta+1}{6\beta}<a\leqslant-\frac{1}{6\beta}$	$v_{ds}\|_{z_1=z_e}\leqslant v_{ds}\leqslant v_{ds}\|_{z_1=0}$
$\beta<0$	$a<-\frac{8c\beta+1}{6\beta}$	$v_{ds}\|_{z_1=0}\leqslant v_{ds}\leqslant v_{ds}\|_{z_1=\pi}$
	$a>\frac{8c\beta-1}{6\beta}$	$v_{ds}\|_{z_1=\pi}\leqslant v_{ds}\leqslant v_{ds}\|_{z_1=0}$
	$-\frac{1}{6\beta}\leqslant a<\frac{8c\beta-1}{6\beta}$	$v_{ds}\|_{z_1=\pi}\leqslant v_{ds}\leqslant v_{ds}\|_{z_1=z_e}$
	$-\frac{8c\beta+1}{6\beta}<a\leqslant-\frac{1}{6\beta}$	$v_{ds}\|_{z_1=0}\leqslant v_{ds}\leqslant v_{ds}\|_{z_1=z_e}$

A. The velocity ranges

We start with one SVDS solution of Eq. (1), with choosing $n=1$ of Eq. (A5),

$$q^{[1]}=\left\{\kappa_1+i\sqrt{c^2-\kappa_1^2}\tanh\left[\sqrt{c^2-\kappa_1^2}(x-v_1t+\gamma_1)\right]\right\}e^{i\theta}, \quad (2)$$

with $\kappa_1=c\cos z_1$, $\kappa_1\in(-c,c)$. γ_1 is the position of SVDS in the distribution direction. $v_1=v_{ds}+a$ is the sum of the soliton velocity and the background velocity, where the soliton velocity is

$$v_{ds}=\beta\left(4\kappa_1^2-6a\kappa_1+3a^2+2c^2\right)-\kappa_1, \quad (3)$$

As it can be seen, the v_{ds} is a quadratic function of κ_1, so the upper and lower speed limits are changed with β and a, as summarized in Table I. With fixing the sign of β, the ranges of v_{ds} can be categorized into four classes according to the regions of wave number a, because the HE does not have the Galilean symmetry. On the contrary, for an SVDS in NLSE, the soliton velocity is independent of the wave number (i.e., for $\beta=0$, $|v|<c$), which the Galilean transformation can remove. Unlike the dark soliton, the velocity of bright soliton in HE is inversely proportional to the strength of high-order effects, so its velocity range is unrestricted [17,27,35]. For the other nonlinear waves in HE, such as rational solutions and breathers, the background wave number affects the velocity value of nonlinear waves rather than the velocity range [29,36].

As we mentioned, the input pulse containing a continuous changing phase can create a moving dark soliton. Thus, there is a close connection between the velocity and phase shift. For a dark soliton in NLSE, there is a one-to-one correspondence between the velocity and phase shift [13]. The discussions of the velocity properties imply that both the high-order effects and background wave number will be crucial to the phase shift of a single dark soliton in HE. This motivates us to study its phase properties.

B. Two correspondence relations between velocity and phase shift

Based on Eq. (2), the phase shift of an SVDS can be exactly calculated as $\Delta\phi = \phi(x \to +\infty) - \phi(x \to -\infty) = 2\arctan(\sqrt{c^2 - \kappa_1^2}/\kappa_1)$, $\Delta\phi \in [-\pi, \pi]$. By combining it with Eq. (3), the correspondence relations between the velocity and phase shift of an SVDS in HE take the following forms:

$$v_{\rm ds} = \beta[4 + 3a^2 + 2\cos(\Delta\phi)] - \cos\left(\frac{\Delta\phi}{2}\right)(6a\beta + 1), \quad \text{for } 0 \leqslant \Delta\phi \leqslant \pi, \tag{4a}$$

$$v_{\rm ds} = \beta[4 + 3a^2 + 2\cos(\Delta\phi)] + \cos\left(\frac{\Delta\phi}{2}\right)(6a\beta + 1), \quad \text{for } -\pi \leqslant \Delta\phi \leqslant 0, \tag{4b}$$

The velocity is codetermined by $\Delta\phi$, a and β. Surprisingly, we find that there are two types of corresponding relations between the phase shift and the velocity for an SVDS (as shown in Fig. 1):

(1) Type I: There is a one-to-one match between the phase shift and velocity for an SVDS, which is similar to that in NLSE.

(2) Type II: There is a two-to-one correspondence relation between the phase shift and velocity for an SVDS, which is not admitted in NLSE.

These indicate that the phase properties for an SVDS with higher-order effects will be more abundant than the one with only the second-order dispersion and self-phase modulation.

We first look briefly at variations of soliton velocity with phase shift by taking $\beta = -0.3$ and $a = 0$, as shown in Fig. 1(a1) with the solid blue curve. For comparative analysis, we also show the case of $\beta = 0$ (i.e., NLSE) with a black dashed-dotted curve. Obviously, even if the background wave number is not considered, the variations of the soliton velocity with phase shift in HE are quite distinct from that of dark solitons in NLSE, where the relation between the velocity and phase shift is a one-to-one correspondence. Particularly, there exists a critical phase shift $\Delta\phi_{c_1}$ marked by the red triangle symbol between two types of correspondence relations. It is seen that only when $\Delta\phi \in (0, \Delta\phi_{c_1})$, the function $v_{\rm ds}(\Delta\phi)$ is injective, thus the relation between the phase shift and velocity satisfies the type I. However, this feature no longer holds in the regions $\Delta\phi \in [-\pi, 0] \cap [\Delta\phi_{c_1}, \pi]$, where two distinct phase shifts can bring about an SVDS with the same velocity. This two-to-one match between the phase shift and velocity is type II, which has never been reported in previous literature.

Moreover, the type II includes two subtypes (denoted as type II-A and type II-B), which are distinguished by the second critical phase shift $\Delta\phi_{c_2}$ marked as the left red triangle symbol, as shown in Fig. 1(a2). For the type II-A, $\Delta\phi \in [-\pi, \Delta\phi_{c_2}]$, the two distinct phase shifts are the same in sign but different in value for an SVDS at the same velocity. While for the type II-B, $\Delta\phi \in (\Delta\phi_{c_2}, 0] \cap [\Delta\phi_{c_1}, \pi]$, both the values and the signs of two phase shifts of an SVDS at the same velocity are different.

More interestingly, we find that background wave number a and coefficient of high-order effects β significantly affect the existence regions of type I and II. For example, we demonstrate the changes of soliton velocity with phase shift and background wave number in Fig. 1(b1) by fixing $\beta = -0.3$. The areas surrounded by white curves are type II, and outside these areas is the type I. It is shown that the type II can emerge when the background wave number $a \in (-\frac{1}{9}, \frac{11}{9})$ and the phase shift in some ranges. The first critical phase shift $\Delta\phi_{c_1}$ between the type I and type II varies with the background wave number. For $a \in (-\frac{1}{9}, \frac{5}{9})$, we get $\Delta\phi_{c_1} = 2\arctan[\frac{\sqrt{(5-9a)(7+9a)}}{9a+1}]$; for $a \in [\frac{5}{9}, \frac{11}{9})$, we obtain $\Delta\phi_{c_1} = 2\arctan[\frac{\sqrt{(17-9a)(9a-5)}}{9a-11}]$. We also present the corresponding two subtypes of type II in Fig. 1(b2). For this case, the type II-A (yellow regions) and type II-B (cyan regions) are distinguished by the second critical phase shift $\Delta\phi_{c_2} = 2\arctan[\frac{\sqrt{(11-9a)(1+9a)}}{9a-5}]$.

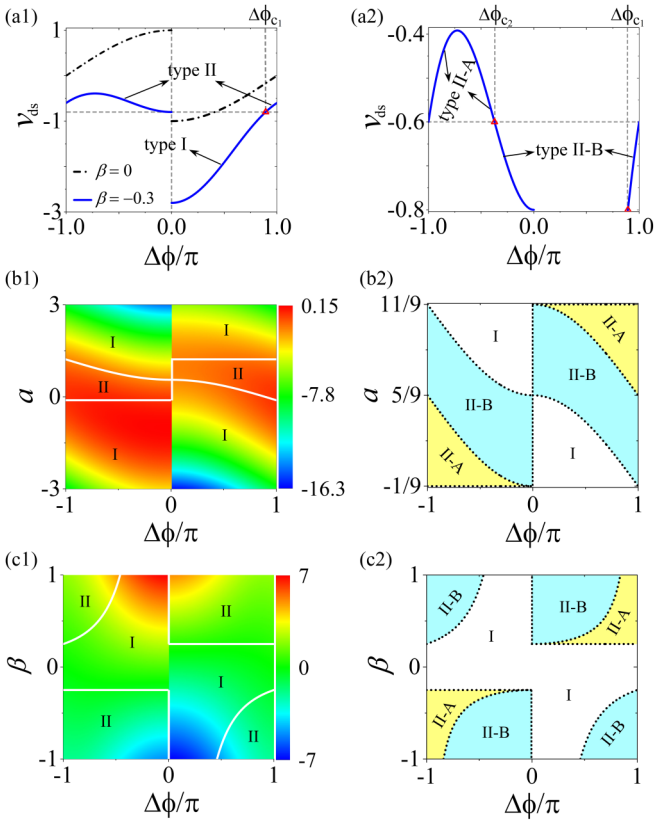

FIG. 1. Two types of correspondence relations between the phase shift ($\Delta\phi$) and velocity ($v_{\rm ds}$) for an SVDS in HE. (a1) The variations of velocity with phase shift. The solid blue curves are obtained with $a = 0$ and $\beta = -0.3$, and the dashed black dotted curves are given by $\beta = 0$. The red symbol denotes the first critical phase shift between type I and II, $\Delta\phi_{c_1} = 2\arccos(1/6)$. (a2) The corresponding two subtypes of type II. The second critical phase shift between two subtypes is $\Delta\phi_{c_2} = -2\arccos(5/6)$. (b1) The variations of soliton velocity $v_{\rm ds}$ vs phase shift $\Delta\phi$ and background wave number a with fixing $\beta = -0.3$. (b2) Phase diagram for the two subtypes of type II shown in panel (b1). (c1) The change of soliton velocity $v_{\rm ds}$ vs phase shift $\Delta\phi$ and high-order effects β with fixing $a = 0$. (c2) Phase diagram for the two subtypes of type II depicted in panel (c1). In panels (b1) and (c1), type II exists in the regions surrounded by solid white curves. The outside of these regions is the type I. In the phase diagrams panels (b2) and (c2), type II-A and type II-B is presented by yellow and cyan regions, respectively.

We further study the impact of the high-order effects on the correspondence relations between the phase shift and soliton velocity by fixing $a = 0$. The result has been shown in Fig. 1(c1). Since the high-order effects are usually weak, we consider $\beta \in [-1, 1]$ herein. For this case, the type II can exist when $\beta \in [-1, \frac{1}{4}) \cap (\frac{1}{4}, 1]$ (existent regions are surrounded by white lines). We also give the phase diagram Fig. 1(c2) to show the corresponding two subtypes of type II in more detail. When $\beta \in [-1, -\frac{1}{4})$, two related critical phase shifts are $\Delta\phi_{c_1} = -2\arctan(\frac{\sqrt{-1-8\beta}}{1+4\beta})$ and $\Delta\phi_{c_2} = -2\arctan(\sqrt{16\beta^2-1})$. When $\beta \in (\frac{1}{4}, 1]$, we get $\Delta\phi_{c_1} = 2\arctan(\frac{\sqrt{-1+8\beta}}{1-4\beta})$ and $\Delta\phi_{c_2} = 2\arctan(\sqrt{16\beta^2-1})$.

The above analyses clearly illustrate that an SVDS with the same velocity can correspond to two distinct phase shifts under certain conditions in HE, in sharp contrast to the one with only the second-order dispersion and self-phase modulation, which admits a one-to-one match between the velocity and phase shift. Recently, the topological phases of nonlinear waves such as dark solitons [13,14], bright solitons [37], rogue waves, and breathers [38] have garnered much attention. It was demonstrated that phase shift is determined solely by the topological vector potential defined in an extended complex plane. It inspires us to investigate the topological vector potentials underlying the distinct phase shifts to further understand the phase characters of an SVDS in the type II region, by utilizing the topological vector potential theory proposed in Refs. [13,38] directly.

C. The topological vector potential underlying the phase shift

We focus on the phase variation of wave function $q^{[n]}$ with leaving out the background's phase $e^{i\theta}$, which can be described by $\phi = \arctan[\frac{\mathrm{Im}(q^{[n]}e^{-i\theta})}{\mathrm{Re}(q^{[n]}e^{-i\theta})}] + k\pi$. Here k is an integer which is determined by phase gradient flow $F(x) = \partial_x\phi$. Then, the wave function $q^{[n]}$ can be expressed in exponential form $q^{[n]} = |q^{[n]}|e^{i\phi}$. By substituting it into the model Eq. (1), we can get the equation $\frac{\partial|q^{[n]}|^2}{\partial t} = -\frac{\partial(|q^{[n]}|^2F(x))}{\partial x} - 3\beta\frac{\partial(|q^{[n]}|^2(F(x))^2)}{\partial x} - 3\beta\frac{\partial|q^{[n]}|^4}{\partial x} + 2\beta|q^{[n]}|\frac{\partial^3|q^{[n]}|}{\partial x^3}$, based on the imaginary part. Then, by conducting the integral over x, the relations between $F(x)$ and intensity $|q^{[n]}|$ can be derived as $F(x) = \frac{-|q^{[n]}|\pm\sqrt{|q^{[n]}|^2+12\beta(g_2-g_1)}}{6\beta|q^{[n]}|}$, where $g_1 = \int\frac{\partial|q^{[n]}|^2}{\partial t}\mathrm{d}x$ and $g_2 = (2\int|q^{[n]}|\frac{\partial^3|q^{[n]}|}{\partial x^3}\mathrm{d}x - 3|q^{[n]}|^4)\beta$, we can know that the intensity zero points can bring the singularities of $F(x)$, which could be used to uncover the topology underlying phase shift. Notably, the intensity zeros for dark soliton with moving speed usually exist on a complex plane. Then, we introduce a function $F(z)$, which is obtained by extending the real coordinate variable x of $F(x)$ to complex coordinate space $z = x + iy$. The existence of the intensity zero points ($|q^{[n]}(\tilde{z}_N)| = 0$) implies that $F(z)$ might have N singularities on the complex plane (marked as $\tilde{z}_N = x_N + iy_N$, N is an integer). Our calculations on all dark solitons here indicate that these singularities are all the first-order ones. Then, based on the Mittag-Leffler theorem [39], the meromorphic function $F(z)$ can be expressed in terms of these singularities, that is, $F(z) = F(0) + \sum_N \mathrm{Res}[F(\tilde{z}_N)](\frac{1}{z-\tilde{z}_N} + \frac{1}{\tilde{z}_N})$. In particular, there is $F(0) + \sum_N\frac{\mathrm{Res}[F(\tilde{z}_N)]}{\tilde{z}_N} = 0$ for these dark solitons. Therefore, we get $F(z) = \sum_N\frac{\mathrm{Res}[F(\tilde{z}_N)]}{z-\tilde{z}_N}$. $\mathrm{Res}[F(\tilde{z}_N)] = \Omega/(i2\pi)$ is residue, with $\Omega = \pm\pi$. Since we focus on the phase character, we define a real vector potential $\mathbf{A}$ on the (x, y) plane [13,38], which can be written as

$$\mathbf{A} = \sum_N \frac{\Omega[(x-x_N)\boldsymbol{j} - (y-y_N)\boldsymbol{i}]}{2\pi[(x-x_N)^2 + (y-y_N)^2]}, \tag{5}$$

Here, $\mathbf{A}$ takes the form of a topological vector potential [40], where $\boldsymbol{i}$ and $\boldsymbol{j}$ are the unit vectors in the x and y directions, respectively. This implies that the effective magnetic field will be zero everywhere in the whole plane except for those singularities. Then, we get

$$\mathbf{B} = \boldsymbol{k}\sum_N \Omega\delta(\boldsymbol{r} - \boldsymbol{r}_N), \tag{6}$$

where $\boldsymbol{r} = x\boldsymbol{i} + y\boldsymbol{j}$, $\boldsymbol{r}_N = x_N\boldsymbol{i} + y_N\boldsymbol{j}$, and $\boldsymbol{k}$ is a unit vector perpendicular to the (x, y) plane. Surprisingly, the magnetic flux of a circle around each pointlike magnetic field on the (x, y) plane is always $\pm\pi$, and $\pm$ is the direction of the magnetic flux. Then the vector field around each singularity can be regarded as "a vortex carrying quantized magnetic flux." Since the topological vector potential is very similar to the ones for the virtual magnetic monopoles in momentum space of topological materials [41], and parameter space of Berry phase theory [42], we term pointlike magnetic fields as the virtual magnetic monopoles in our result. The phase variations can be described by the integration of the vector potential $\mathbf{A}$ along the real x axis, that is, $\Delta\phi = \phi(x \to +\infty) - \phi(x \to -\infty) = \int_{-\infty}^{+\infty}\mathbf{A}(x, y = 0)\cdot\boldsymbol{i}\mathrm{d}x$. Then, we can explore the topological phases of n-dark solitons by performing above topological theory on the dark soliton solution $q^{[n]}$ in HE.

Now we characterize the topology of the SVDS. For this case, we get $F(z) = \frac{2\kappa_1(c^2-\kappa_1^2)}{2\kappa_1^2-c^2+c^2\cosh(2\sqrt{c^2-\kappa_1^2}z)}$. Then, the vector potential $\mathbf{A}$ is determined by the singularities in the complex plane,

$$\tilde{z}_N : x_N = 0, \quad y_N = \pm y_0 + NT \quad (N = 0 \pm 1, \ldots), \tag{7}$$

where $y_0 = \frac{\mathrm{arccosh}[2(c^2-\kappa_1^2)-1]}{2\sqrt{c^2-\kappa_1^2}}$ and the period $T = \frac{\pi}{\sqrt{c^2-\kappa_1^2}}$. Then, we describe the topological property of an SVDS in the regime of type II. For example, we exhibit the topological phase of an SVDS with $v_{\mathrm{ds}} = -0.74$. The related two different topological phases have been presented Figs. 2(a1), 2(a2) and 2(b1), 2(b2), respectively. The topological vector potentials $\mathbf{A}$ are shown in the left panel, and the corresponding phase distributions ϕ (solid curve) are depicted in the right panel. Obviously, the topological vector potential in Fig. 2(a1) is quite distinct from the one in Fig. 2(b1), involving the position, period, and the direction of the magnetic fluxes. Consequently, the different topological vector potentials give rise to the different phase profiles. The phase distribution of Fig. 2(a1) is shown in Fig. 2(a2), with phase shift about $\Delta\phi = -0.19\pi$. For Fig. 2(b1), the resulting phase shift is about $\Delta\phi = 0.92\pi$, as shown in Fig. 2(b2). The coordinates of virtual monopoles and the phase shift value are accurate to two decimal places in our results.

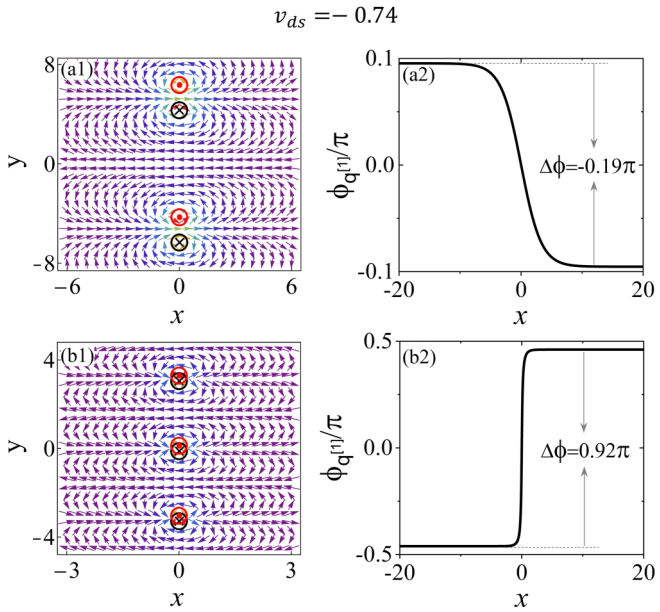

FIG. 2. Two different topological phases for an SVDS with the same velocity $v_{\rm ds} = -0.74$ in HE. Left panel: the topological vector potential **A**. The virtual magnetic monopoles with $+\pi$ $(-\pi)$ magnetic fluxes are shown by the red symbols $\odot$ (black symbols $\otimes$). The paired virtual monopoles are located at (0 ± 4.31) for (a1) and (0 ± 0.12) for (b1) with a period $T = \pi/\sqrt{c^2 - \kappa_1^2}$ along the imaginary axis y. Right plane: the corresponding phase distribution. (a1, a2): $\Delta\phi = -0.19\pi$, $\kappa_1 = -(25 + \sqrt{1045})/60$. (b1, b2): $\Delta\phi = 0.92\pi$, $\kappa_1 = -(25 - \sqrt{1045})/60$. The other parameters are $c = 1, a = 0, \beta = -0.3, \gamma_1 = 0$.

The above results indicate that two parallel SVDSs can be obtained when two SVDSs are in the regions of type II, where SVDSs with the same velocity have two different phase shifts, which can physically explain the generation mechanism of previously reported DVDSs and parallel SVDSs in HE [20,23,24]. Based on the abundant phase characters of the SVDS demonstrated above, we can expect that the phase properties of DVDS will be more attractive in HE.

III. THE PHASE CHARACTERS OF A DOUBLE-VALLEY DARK SOLITON

A general DVDS solution in compact form is given by

$$q^{[2]} = c\frac{\varrho^2 e^{-\eta_1-\eta_2} + e^{\eta_1+\eta_2} + 2\cosh(\eta_1-\eta_2)}{\varrho^2 e^{-\xi_1-\xi_2} + e^{\xi_1+\xi_2} + 2\cosh(\xi_1-\xi_2)} e^{i\theta}, \quad (8)$$

where $\varrho = \sin[(z_1 - z_2)/2]/\sin[(z_1 + z_2)/2]$, $\eta_i = \xi_i + iz_i$, $\xi_i = c\sin(z_i)(x - v_1 t + \gamma_i)$, $i = 1, 2$. Two free parameters γ_1 and γ_2 are introduced to adjust the overlap degree between two valleys of DVDS.

The detailed derivation processes for DVDS have been presented in Appendix A. To clearly understand the velocity feature of DVDS, we carefully calculate the velocity ranges of DVDS by satisfying the constraint conditions Eq. (A7) and Eq. (A8). The results have been summarized in Table II. Recently, it was reported that the width-dependent parameters of solitons significantly affect the velocity ranges of DVDS in the Manakov model [14]. On the contrary, the velocity

TABLE II. The velocity ranges of a DVDS. The explicit expressions of $v_{\rm ds}|_{z_1=z_e}$, $v_{\rm ds}|_{z_1=0}$, and $v_{\rm ds}|_{z_1=\pi}$ have been given in Table I.

β	a	z_1	$v_{\rm ds}$
$\beta > 0$	$\left[-\frac{1}{6\beta}, \frac{8c\beta-1}{6\beta}\right)$	$[0, \arccos(\rho - 1)]$	$[v_{\rm ds}\|_{z_1=z_e}, v_{\rm ds}\|_{z_1=\pi}]$
	$\left(\frac{-8c\beta-1}{6\beta}, -\frac{1}{6\beta}\right)$	$[\arccos(\rho + 1), \pi]$	$[v_{\rm ds}\|_{z_1=z_e}, v_{\rm ds}\|_{z_1=0}]$
$\beta < 0$	$\left[-\frac{1}{6\beta}, \frac{8c\beta-1}{6\beta}\right)$	$[0, \arccos(\rho - 1)]$	$[v_{\rm ds}\|_{z_1=\pi}, v_{\rm ds}\|_{z_1=z_e}]$
	$\left(\frac{-8c\beta-1}{6\beta}, -\frac{1}{6\beta}\right)$	$[\arccos(\rho + 1), \pi]$	$[v_{\rm ds}\|_{z_1=0}, v_{\rm ds}\|_{z_1=z_e}]$

ranges of DVDS in HE depend on the high-order nonlinearity coefficient and background wave number. Generally, the intensity profile of DVDS is asymmetric. In particular, when two free parameters γ_1 and γ_2 satisfy the relation $\gamma_2 = \gamma_1 + \frac{\sin(z_1)-\sin(z_2)}{2c\sin(z_1)\sin(z_2)}\ln(|\varrho|)$, the DVDS solution Eq. (8) can give a DVDS with a symmetric intensity profile, and the symmetry line is $x = v_1 t - \gamma_1 + \ln[\frac{|\varrho|}{2c\sin(z_1)}]$. For example, we show these two intensity profiles in Figs. 3(a1) and 3(b1), respectively.

We now focus our analysis on the phase characters of the DVDSs. Since the two parallel SVDSs that constitute the DVDS can exist in the region of the type II-A or the type II-B (as shown in Fig. 1), the phase profiles of DVDSs will include two types. One is a double-step type when two parallel SVDSs are in the regime of type II-A, and the other is a U-shaped type when the two parallel SVDSs are in the regime of type II-B. Then, we will investigate these two types of phase properties of DVDS in detail.

Based on the topology of dark solitons, the phase properties of DVDS will be closely related to the underlying topological vector potentials. To facilitate analysis, we make the phase of DVDS remain unchanged at $x \to -\infty$, based on the expression $q^{[2]}(x \to -\infty) = e^{-i(z_1+z_2)+in\pi}$ (n is an

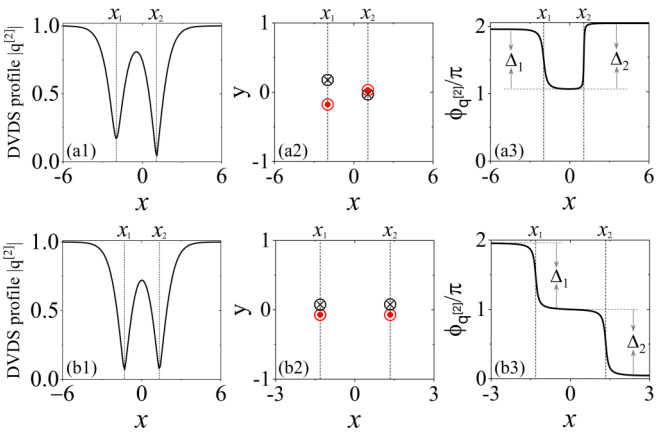

FIG. 3. Top plane: (a1) amplitude distribution, (a2) virtual magnetic monopole fields in the complex plane, and (a3) phase distribution for an asymmetric DVDS ($\gamma_2 = -0.1$). The singularities in panel (a2) are located at (-1.98 ± 0.18), (1.07 ± 0.03). Bottom plane: (b1) amplitude distribution, (b2) virtual magnetic monopole fields in the complex plane, and (b3) phase distribution for a symmetric DVDS ($\gamma_2 = -1.02$). The singularities in panel (b2) are located at (-1.31 ± 0.07), (1.34 ± 0.07). The other parameters are $a = 0.742485$, $c = 1$, $\beta = -0.2$, $z_1 = 1.5$, $z_2 = 1.77931$, $\gamma_1 = -1$.

arbitrary integer). For example, we demonstrate the phase characteristics of the DVDSs shown in Figs. 3(a1) and 3(b1). Their topological magnetic fields associated with the vector potential in (x, y) plane are depicted in Figs. 3(a2)–3(b2). Without loss of generality, we show the virtual monopoles within the region $y \in [1, -1]$. As it can be seen, the paired virtual monopoles in the complex plane are scattered on two separate lines $x = x_1$ and $x = x_2$. The integral of the vector potential corresponding to each line will lead to a phase shift Δ_j at $x = x_j$ for $j = 1, 2$. The sum of two phase shifts gives the total phase shift of a DVDS.

It is noteworthy that, for the asymmetric DVDS, the magnetic flux direction of the virtual monopoles on the two lines is opposite, which gives rise to the opposite sign of the phase shift on the line x_1 and the one on the line x_2, and form a U-shaped phase profile, as shown in Figs. 3(a2) and 3(a3). Therefore, this DVDS consists of two SVDSs in the regime of the type II-B mentioned in Fig. 1. Moreover, the virtual monopoles on the $x = x_2$ line are quite close to each other, resulting in a sharp phase shift Δ_2 closer to π. We numerically obtain the associated phase shifts are $\Delta_1 = -0.89\pi$ and $\Delta_2 = 0.97\pi$. Therefore, the total phase shift of the asymmetric DVDS is $\Delta\phi = \Delta_1 + \Delta_2 = 0.08\pi$.

On the contrary, for the symmetric DVDS, the magnetic flux direction of the virtual monopoles on line $x = x_1$ is the same as that of the ones on line $x = x_2$, as shown in Fig. 3(b2). Therefore, this DVDS is composed of two SVDSs in the regime of the type II-A mentioned in Fig. 1. Moreover, two pairs of monopoles are distributed symmetrically in the (x, y) plane, so the associated two phase steps are the same, $\Delta_1 = \Delta_2 = -0.96\pi$. Thus, the total phase shift of the symmetric DVDS is $\Delta\phi = \Delta_1 + \Delta_2 = -1.92\pi$. The phase distribution exhibits an apparent double-step structure, as shown in Fig. 3(b3), which is similar to that of the DVDS obtained in Manakov systems [13,14].

The above results have demonstrated that the DVDS with the same velocity can also have two types of phase profiles, by changing the intensity profiles adjusted by two free parameters γ_1 and γ_2, as shown in Fig. 2. For example, we give a phase diagram for two types of phase characters by changing parameters γ_1 and γ_2, and the other parameters are identical to the ones in Fig. 3. The results have been presented in Fig. 4, which is obtained by judging the sign of the phase gradient flow $F[x]$ numerically. The triangle and circle symbols correspond to Figs. 3(a3) and 3(b3), respectively. As it can be seen, double-step type phase distribution exists only in narrow parameter space, among which the solid black line corresponds to the symmetric DVDS. This means the symmetric DVDS always possesses the double-step type phase distribution, while the phase distribution of asymmetric DVDS can be U-shaped type or double-step type. The critical states between these two types are related to the density zeros of the DVDS in real space. This diagram also indicates that nearly identical intensity profiles of a DVDS with identical velocity can possess two distinct topological properties in adjacent areas of the two types. However, the topological phase and the velocity of the DVDS in the Manakov system can only be one-to-one correspondence [13,14]. Our results provide some important complements for understanding the phase properties of dark solitons.

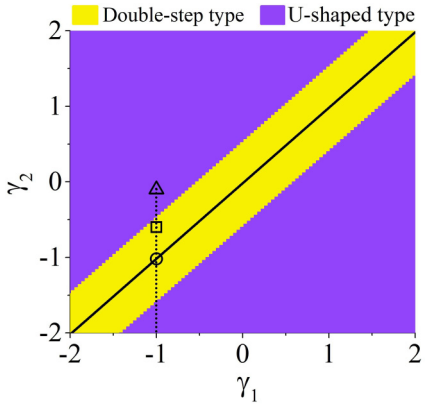

FIG. 4. A phase diagram for two types of phase profiles for DVDS. The yellow region represents to the double-step type, and the purple region stands for the U-shaped type. The black solid line correspond to the symmetric DVDS. The triangle and circle symbols correspond to Figs. 3(a3) and 3(b3), respectively. The parameters are same as Fig. 3 (excepting γ_1 and γ_2). This picture also describes the phase properties of DVDS before colliding with SVDS, in which the square symbol is related to the DVDS ("S_2" soliton) shown in Fig. 5.

IV. PHASE VARIATIONS OF DVDS INDUCED BY THE COLLISION

Previous studies of solitons' collision were mainly focused on the interactions between two solitons by analyzing the variations of their intensity profiles, but the collision properties between arbitrary n-dark solitons have never been considered due to some mathematical difficulties [14,23,33,43–51]. However, solitons' phase characters during a collision process have never been considered. In this section, we will investigate the collision properties containing n_1 SVDSs and n_2 DVDSs by analyzing their phase properties, expecting that phase characteristics can help to identify the collision properties through an alternative way. To get an accurate and direct analysis, the premise is to get the simple and compact asymptotic expressions ($t \to \pm\infty$) before and after the collision. To this end, we for the first time present the systematic and detailed asymptotic analyses for n-dark solitons involving n_1 SVDSs and n_2 DVDSs ($n = n_1 + 2n_2$) in Appendix B, by developing the asymptotic analysis technique and performing onerous calculations. The n-dark solitons are ranked by the whole velocities, supposing $v_1 \leqslant \cdots \leqslant v_k \leqslant \cdots \leqslant v_n$ $(k = 1, \ldots, n)$. Their collisions can be inelastic or elastic under different conditions. The inelastic collisions make the intensity and phase profiles change of DVDSs, while there is no change for the SVDS.

For example, without loss of generality, we consider the collision between one SVDS ($n_1 = 1$) and one DVDS ($n_2 = 1$) in the following, based on the solution $q^{[3]}$ Eq. (A5) with assuming $v_2 = v_1 < v_3$. On account of Eqs. (B2) and (B3), the asymptotic expressions of SVDS solution q_{s_1} before and after the collision are given in the following form:

$$q_{s_1}^{\pm} = cL_{s_1}^{\pm}[1 - B_3 + B_3 \tanh(Y_{s_1}^{\pm})]e^{i\theta}, \tag{9}$$

where

$$L_{s_1}^{-} = e^{-2i(z_1+z_2)},\ L_{s_1}^{+} = 1,\ K_1^{-} = \omega_{[3,1]}\omega_{[3,2]},\ K^{+} = 1,$$
$$Y_{s_1}^{\pm} = c\sin z_3(x - v_3 t + \gamma_3) - \ln|K_1^{\pm}|,\ B_3 = i\sin z_3 e^{-iz_3}.$$

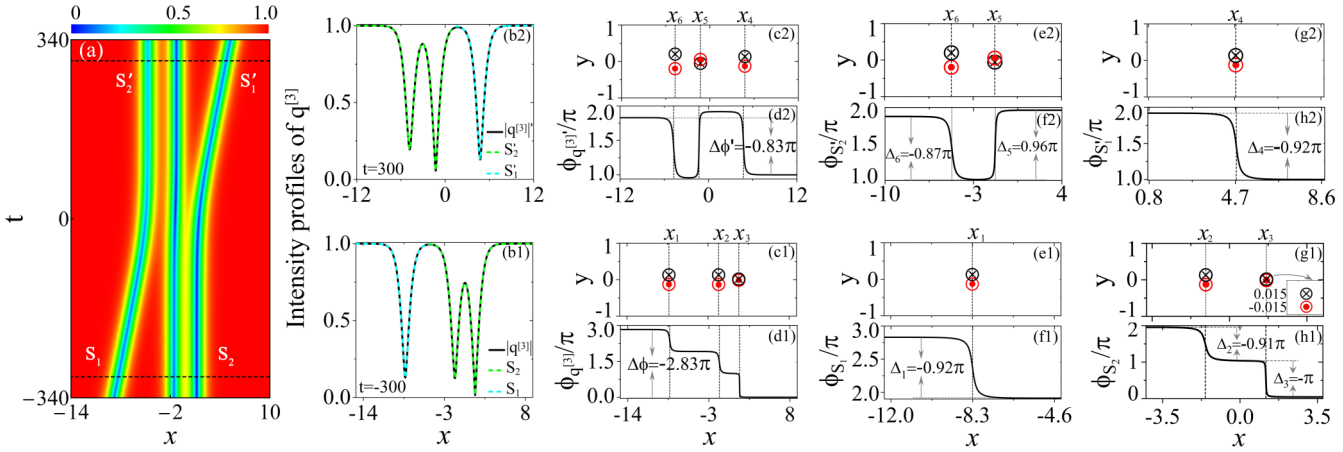

FIG. 5. An inelastic collision between an asymmetric DVDS and an SVDS. Before (after) the collision, the SVDS, the DVDS and two solitons solution are marked as "S_1," "S_2," and "$q^{[3]}$" ("S_1'," "S_2'," and "$q^{[3]'}$"), respectively. (a) Temporal-spatial intensity distribution. (b1, b2) Intensity profiles of two solitons before ($t=-300$) and after ($t=300$) collision. The solid black curve, dashed cyan curve, and dashed green curve is plotted by the solution $q^{[3]}$, the asymptotic expression Eq. (9) of SVDS and Eq. (10) of DVDS, respectively, at the fixed t. (c1–h1) Virtual magnetic monopole fields and the corresponding phase profiles of $q^{[3]}$, "S_1," and "S_2," respectively. The singularities on the line $x=x_1$, $x=x_2$, and $x=x_3$ are located at (-8.31 ± 0.13), (-1.57 ± 0.13), and (1.17 ± 0.02), respectively. (c2–h2) Virtual magnetic monopole fields and the corresponding phase distributions of "$q^{[3]'}$," "S_2'," and "S_1'," respectively. The singularities on the line $x=x_6$, $x=x_5$, and $x=x_4$ are located at (-4.72 ± 0.20), (-1.28 ± 0.05), and (4.74 ± 0.13), respectively. It is seen that both the phase characteristic and intensity profile of the DVDS change remarkably after colliding with SVSD. However, nothing has changed on the latter. The parameters are $c=1$, $\beta=-0.2$, $a=0.742485$, $d=1$, $z_1=1.5$, $z_2=1.77931$, $z_3=1.7$, $\gamma_1=-1$, $\gamma_2=-0.6$, $\gamma_3=-1$.

The superscript "$\pm$" in the top right-hand corner represents the asymptotic form of soliton after ($t\to+\infty$) and before ($t\to-\infty$) colliding with SVDS. Based on the asymptotic analysis results Eqs. (B5) and (B6), the asymptotic behaviors of the DVDS can be described by the solution q_{s_2}, which is given by

$$q_{s_2}^{\pm}=cL_{s_2}^{\pm}\frac{N_{s_2}^{\pm}}{D_{s_2}^{\pm}}e^{i\theta}, \tag{10}$$

where

$$N_{s_2}^{\pm}=K_2^{\pm}e^{-\eta_1-\eta_2}+K_3^{\pm}e^{\eta_1-\eta_2}+K_4^{\pm}e^{\eta_2-\eta_1}+e^{\eta_1+\eta_2},$$
$$D_{s_2}^{\pm}=K_2^{\pm}e^{-\xi_1-\xi_2}+K_3^{\pm}e^{\xi_1-\xi_2}+K_4^{\pm}e^{\xi_2-\xi_1}+e^{\xi_1+\xi_2},$$

and

$$K_2^{-}=\omega_{[1,2]}^2,\quad K_2^{+}=\omega_{[1,2]}^2\omega_{[1,3]}^2\omega_{[2,3]}^2,$$
$$K_3^{-}=1,\quad K_3^{+}=\omega_{[2,3]}^2,\quad K_4^{-}=1,\quad K_4^{+}=\omega_{[1,3]}^2,$$
$$L_{s_1}^{-}=1,\quad L_{s_1}^{+}=e^{-2iz_3},\quad \omega_{[j,i]}=\frac{\sin\left[\frac{(z_j-z_i)}{2}\right]}{\sin\left[\frac{(z_j+z_i)}{2}\right]}.$$

Above explicit asymptotic expressions provide the most crucial conditions to analyze collision properties exactly and comprehensively.

A. Inelastic collision

We start with the inelastic interaction between one DVDS and one SVDS. For example, we show their spatial-temporal intensity distribution in Fig. 5(a) with $v_1=0$ and $v_3=0.0125$. Before (after) the collision, two solitons, the SVDS and DVDS are marked as "$q^{[3]}$" ("$q^{[3]'}$"), "S_1" ("S_1'"), and "S_2" ("S_2'"), respectively. The black dashed lines in upper and lower Fig. 5(a) are used to represent the final state ($t=300$) and initial state ($t=-300$) of two solitons. We will analyze the intensity profiles and phase distributions of solitons in these two states. Figures 5(b1) and 5(b2) are the intensity profiles before and after the collision, in which the black solid curve, cyan dashed curve, and green dashed curve is plotted based on the solution $q^{[3]}$, $q_{s_1}^{\pm}$, and $q_{s_2}^{\pm}$, respectively. It is seen that after the collision, the depths of two valleys of DVDS have changed dramatically, while the intensity profile of SVDS remains unchanged. To analyze and understand the interaction process comprehensively and deeply, the investigations of phase properties of two solitons before and after the collision are also indispensable. Then, we will conduct the complex extending on expressions Eqs. (A5), (9), and (10) to analyze their topological properties, based on the topological vector potential theory mentioned in Sec. II C.

Before (after) the collision, the phase characteristics of $q^{[3]}$ ($q^{[3]'}$), "S_1" ("S_1'"), and "S_2" ("S_2'") have been presented in Figs. 5(c1)–5(h1) [Figs. 5(c2)–5(h2)]. In these graphs, the topological magnetic fields in complex space are depicted by some pointlike symbols, and solid black curves present the corresponding phase distributions. Interestingly, the phase profile of two solitons initially presents a triple-step structure in one direction, as shown in Fig. 5(d1). Surprisingly, when two solitons accomplish the collision process, the phase distribution becomes a more complex structure composed of three phase shifts in different directions, as shown in Fig. 5(d2). This dramatic change in the phase distribution originates from the underlying topological potentials. The virtual magnetic monopoles are scattered on three separate lines at $x=x_1$, $x=x_2$, and $x=x_3$ before the collision, as exhibited in Fig. 5(c1) [$x=x_4$, $x=x_5$, and $x=x_6$ after the collision, as exhibited in Fig. 5(c2)] along the imaginary axis. For simplicity, we show the paired virtual monopoles on the line x_j when the imaginary axis $y\in[1,-1]$ in this section. Strikingly, the magnetic fluxes directions at these three pairs of virtual monopoles are

the same before the collision, while that of one is reversed after the collision, compared to Fig. 5(c2) with Fig. 5(c1). This motivates us to explore what happened in each of the solitons.

We show the virtual monopole fields and the corresponding phase distributions of the SVDS before and after collision in Figs. 5(e1)–5(f1) and 5(g2)–5(h2). It is seen that SVDS maintains a single-step structure. Before the collision, virtual monopoles are located on the line $x = x_1$, and the associated phase shift is $\Delta_1 = -0.92\pi$. Then, they move to the line $x = x_4$ after the collision. Obviously, there is only a translation in the x axis for these virtual monopoles. Consequently, the phase shift is $\Delta_4 = \Delta_1 = -0.92\pi$. Therefore, the intensity profile and phase feature of SVDS can be held well after interacting with DVDS.

However, the topological phase of DVDS undergoes a dramatic change, comparing Figs. 5(g1)–5(h1) with Figs. 5(e2)–5(f2). In the initial state, the phase distribution of DVDS is double-step type since the magnetic fluxes directions at two pairs of virtual monopoles are identical, as shown in Figs. 5(g1)–5(h1). The paired virtual monopoles on the line $x = x_2$ contribute to the phase shift $\Delta_2 = -0.91\pi$. Interestingly, the virtual monopoles on the line $x = x_3$ tend to merge in the real axis x, leading to approximately a phase shift $\Delta_3 = -\pi$. Due to the coordinate values along the imaginary axis y being too small to see them separately, we further plot the insert for them in Fig. 5(g1). Then, we can get the total phase shift of DVDS before the collision is $\Delta_2 + \Delta_3 = -1.91\pi$.

Then, we analyze the phase characteristic of DVDS after the collision, as depicted in Figs. 5(e2)–5(f2). Strikingly, the phase distribution of the DVDS is transformed from the double-step type to the U-shaped type. The magnetic flux direction of the paired virtual monopoles on the lines $x = x_6$ and $x = x_5$ are opposite, and these monopoles give rise to $\Delta_6 = -0.87\pi$ and $\Delta_5 = 0.96\pi$. Thus, the total phase shift of DVDS after the collision is $\Delta_6 + \Delta_5 = 0.09\pi$. These suggest that two parallel SVDSs that make up the DVDS are transformed from the region of the type II-A to the type II-B in this collision process. This is an all-important signal of the inelastic collision.

These results imply that the inelastic collision of DVDS can cause a striking transformation between two types of phase characters. Such an intriguing phenomenon has never been observed in previous literature. In our prework Ref. [23], our understanding of the inelastic collision only depends on the variations of intensity profiles, while important phase properties hidden in the change of soliton profiles have been ignored. Then we would like to know whether such phase transition always exists for the collision dynamics involving the DVDS. For this purpose, we intend to establish phase diagrams for the phase characters of the DVDS before and after the collision, which can be realized by judging the sign of the phase gradient flow $F(x)$ of the asymptotic expressions Eq. (10).

For convenience, we choose the parameters identical to the ones in Fig. 5 except for parameters γ_1 and γ_2. Due to $v_1 < v_3$, the asymptotic expressions $q_{s_2}^-$ expressed by Eq. (10) is actually identical to the DVDS solution Eq. (8). It demonstrates that the asymptotic behavior of DVDS before the collision is independent of the SVDS. Meanwhile, owing to the other related parameters z_1, z_2, a, c, and β in Figs. 5 and 3 are the same. Thus, the phase diagram of phase characters for the DVDS before the collision is identical to Fig. 4. The square symbol in Fig. 4 corresponds to the "S_2" soliton exhibited in Fig. 5(a), which admits the double-step type phase distribution, as shown in Fig. 5(h1). Similarly, we further give a phase diagram for the DVDS after the collision, with the aid of the asymptotic expressions $q_{s_2}^+$ expressed by Eq. (10). The results have been presented in Fig. 6, where the square symbol corresponds to the "S_2'" soliton depicted in Fig. 5(a), which admits the U-shaped type phase distribution, as shown in Fig. 5(f2). The black line is the symmetric DVDS after the collision, and the relation between γ_1 and γ_2 is recalculated as $\gamma_2 = \gamma_1 + \frac{[\sin(z_1)-\sin(z_2)]\ln(K_2^+)-[\sin(z_1)+\sin(z_2)][\ln(K_4^+)-\ln(K_3^+)]}{4\sin(z_1)\sin(z_2)}$.

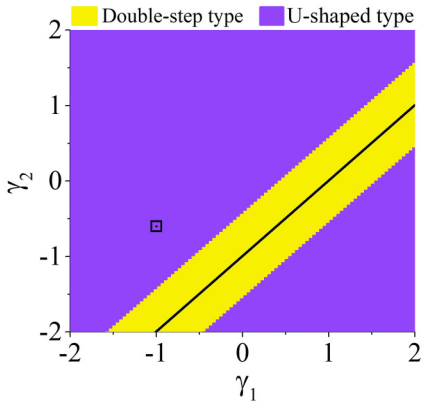

FIG. 6. A phase diagram for the phase properties of DVDS ("S_2'" soliton) after colliding with SVDS, in which the square symbol represents the phase characteristic of "S_2'" soliton shown in Fig. 5. The black line corresponds to the symmetric DVDS. The other parameters are identical to the ones in Fig. 5.

By comparing Figs. 4 and 6, we can see that the existing regions of each type of phase distribution before and after the collision are obviously changed in the (γ_1, γ_2) plane. During a collision process, the phase variations of the DVDS include four kinds: double-step type to U-shaped type, U-shaped type to double-step type, U-shaped type to U-shaped type, and double-step type to double-step type. Remarkably, the symmetric DVDS always keeps the double-step type phase distribution. These results reveal the extraordinary phase properties behind the inelastic collision and further deepen our understanding of solitons collision in essence. It also should be mentioned that Figs. 4 and 6 are not the only phase diagrams. When the other related parameters are varied, the corresponding phase diagram will also be changed.

B. Elastic collision

The above-detailed analysis has revealed the intriguing phase transition of DVDS induced by the inelastic collision. It was reported that the collision of DVDS also could be elastic [23]. Then, we will investigate the phase properties of DVDS that undergo elastic interaction. The elastic collision condition of DVDS has been proved in Appendix C, which is a sufficient condition Eq. (C3). For example, we show the elastic interaction between a DVDS and an SVDS in Fig. 7(a). The meanings of all marks herein are the same as Fig. 5; we

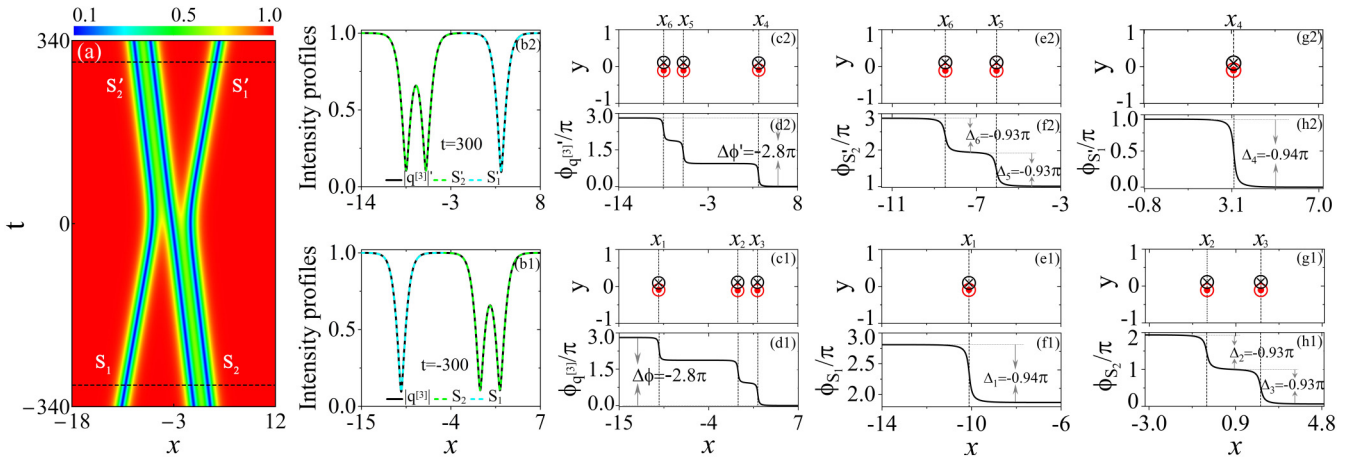

FIG. 7. An elastic collision between a symmetric DVDS and an SVDS. Before (after) the collision, the SVDS, the DVDS and two solitons solution are marked as "S_1," "S_2," and "$q^{[3]}$" ("S_1'," "S_2'," and "$q^{[3]'}$"), respectively. (a) Temporal-spatial intensity distribution. (b1, b2) Intensity profiles before ($t = -300$) and after ($t = 300$) collision. The solid black line, cyan dashed line, and green dashed line are obtained by the two solitons solution Eq. (A5), the asymptotic expression Eq. (9) of SVDS and Eq. (10) of DVDS ($n = 3$), respectively. (c1–h1) Virtual magnetic monopole fields and corresponding phase distributions of $q^{[3]}$, "S_1," and "S_2," respectively. The singularities on the line $x = x_1, x = x_2$, and $x = x_3$ are located at (-10.11 ± 0.10), (-0.40 ± 0.11), and (2.03 ± 0.11), respectively. (c2–h2) Virtual magnetic monopole fields and corresponding phase distributions of $q^{[3]'}$, "S_2'," and "S_1'," respectively. The singularities on the line $x = x_4, x = x_5$, and $x = x_6$ are located at (3.20 ± 0.10), (-6.06 ± 0.11), and (-8.49 ± 0.11), respectively. As can be seen, both the phase properties and intensity profiles of the SVDS and the DVDS have remained the same before and after the collision. The parameters are $c = 1$, $\beta = -0.2$, $a = 0.7$, $d = 1$, $z_1 = 1.5$, $z_2 = 1.84496$, $z_3 = 1.66645$, $\gamma_1 = 1.1$, $\gamma_2 = 1.06812$, $\gamma_3 = 1$.

will not reiterate them. Based on the expressions $q^{[3]}$, Eqs. (9) and (10), and performing the complex extending method, the topological phase of this elastic collision can also be studied well.

The total phase characteristics of two solitons before and after the collision have been shown in Figs. 7(c1)–7(d1) and Figs. 7(c2)–7(d2). It is seen that the magnetic fluxes directions at three pairs of virtual monopoles on three separate lines are consistent before and after the collision so that the phase profiles keep triple-step structures.

The phase feature for the SVDS before and after the collision has been shown in Figs. 7(e1)–7(f1) and Figs. 7(g2)–7(h2). The virtual monopoles on the line x_1 are initially located at (-10.11 ± 0.10). Finally, they are moved to the line $x = x_4$ and are located at (3.20 ± 0.10). Therefore, the topological property of SVDS has remained the same after colliding with DVDS, associated phase shift $\Delta_4 = \Delta_1 = -0.94\pi$.

In this case, the DVDS also admits a similar feature, as shown in Figs. 7(g1)–7(h1) and Figs. 7(e2)–7(f2). Before the collision, two pairs of virtual monopoles are scattered on the lines $x = x_2$ and $x = x_3$, and located at (-0.40 ± 0.11) and (2.03 ± 0.11). After the collision, they are located at (-6.06 ± 0.11) and (-8.49 ± 0.11) on the line $x = x_5$ and $x = x_6$, respectively. Two pairs of virtual monopoles have only undergone a translation along the real axis. This also reveals that the associated two parallel SVDSs are in the regime of type II-A. Moreover, the paired virtual monopoles for the DVDS are symmetrically distributed on (x, y) panel, which leads to a symmetric phase profile. We get $\Delta_2 = \Delta_3 = \Delta_6 = \Delta_5 = -0.93\pi$ numerically, so the total phase shift of DVDS is equal to -1.86π. Then, we can obtain the total phase shift of two solitons is $\Delta\phi = \Delta\phi' = -0.94\pi - 1.86\pi = -2.8\pi$.

These results indicate that we can analyze the phase properties of each soliton to understand and predict the collision properties, combining the succinct asymptotic expressions and topological vector potential. In general, the inelastic interactions of solitons bring variations in both the intensity profiles and topological phase. Similar phenomena can also be observed in the collision between two DVDSs, and even multiple collisions involving the DVDSs, based on the n-dark soliton solution Eq. (A5) and the asymptotic expressions Eqs. (B2)–(B6) for n-dark solitons including n_1 SVDSs and n_2 DVDSs ($n = n_1 + 2n_2$).

V. CONCLUSIONS

We demonstrate that the SVDS with the same velocity can admit two different phase shifts in HE, which can explain the formation mechanism of the DVDS previously reported in HE. Meanwhile, the DVDSs have two types of phase characters. We further uncover the different virtual monopole fields underlying the different phase shifts. Furthermore, we discuss the collision properties of DVDSs from a topological phase standpoint, which has never been reported before. In particular, an inelastic collision can lead to the conversion between two types of phase characters of DVDS. The detailed analyses reveal that the collision properties can be distinguished by analyzing the topological phases, not just intensity profiles. These results provide essential supplements and understandings of dark solitons' phase characters and dynamical properties.

ACKNOWLEDGMENTS

Y.-H. Qin was supported by the China Postdoctoral Science Foundation (Contract No. 2021M701255), and the

National Natural Science Foundation of China (Contract No. 12147170). L.-C. Zhao was supported by the National Natural Science Foundation of China (Contracts No. 12022513 and No. 11775176), and the Major Basic Research Program of Natural Science of Shaanxi Province (Grant No. 2018KJXX-094). Liming Ling is supported by the National Natural Science Foundation of China (Grant No. 12122105) and the Guangzhou Science and Technology Program of China (Grant No. 201904010362).

APPENDIX A: THE DERIVATION OF *n*-DARK SOLITONS SOLUTION

The defocusing HE Eq. (1) admits the following Lax pair:

$$\mathbf{\Phi}_x = \mathbf{U}(\lambda;q)\mathbf{\Phi}, \quad \mathbf{\Phi}_t = \mathbf{V}(\lambda;q)\mathbf{\Phi}, \tag{A1}$$

where λ is real spectral parameter, and

$$\mathbf{U}(\lambda;q) = \begin{bmatrix} i\lambda & -iq^* \\ iq & -i\lambda \end{bmatrix}, \quad \mathbf{V}(\lambda;q) = \begin{bmatrix} V_{1,1} & V_{1,2} \\ V_{2,1} & -V_{1,1} \end{bmatrix},$$

with

$$V_{1,1} = \beta(-4i\lambda^3 - 2i|q|^2\lambda + q_x q^* - q_x^* q) + i\lambda^2 + \frac{i}{2}|q|^2,$$

$$V_{1,2} = \beta(4iq^*\lambda^2 + 2q_x^*\lambda + 2i|q|^2 q^* - iq_{xx}^*) - iq^*\lambda - \frac{1}{2}q_x^*,$$

$$V_{2,1} = \beta(-4iq\lambda^2 + 2q_x\lambda - 2i|q|^2 q + iq_{xx}) + iq\lambda - \frac{1}{2}q_x.$$

To obtain the general solutions of Eq. (1), we start with seed solution $q^{[0]} = ce^{i\theta}$, with $\theta = ax - bt$ and $b = \beta(a^2 + 6c^2)a + \frac{1}{2}a^2 + c^2$. Then utilizing the transformation $\mathbf{B} = \mathrm{diag}(1, e^{-i\theta})$ to convert the variable coefficient differential equation Eq. (A1) into a constant coefficient equation

$$\tilde{\mathbf{\Phi}}_x = i\mathbf{U_1}\tilde{\mathbf{\Phi}}, \quad \mathbf{\Phi} = \mathbf{B}^{-1}\tilde{\mathbf{\Phi}}, \tag{A2a}$$

$$\tilde{\mathbf{\Phi}}_t = i\mathbf{V_1}\tilde{\mathbf{\Phi}} = i(\varepsilon_1\mathbf{U_1} + \varepsilon_2)\tilde{\mathbf{\Phi}}, \tag{A2b}$$

where

$$\mathbf{U_1} = \begin{bmatrix} \lambda & -c \\ c & -\lambda - a \end{bmatrix},$$

$$\varepsilon_1 = \beta(-4\lambda^2 + 2a\lambda - a^2 - 2c^2) + \lambda - \frac{1}{2}a,$$

$$\varepsilon_2 = \beta(-2\lambda^2 + a_1\lambda + 2c^2)a + \frac{1}{2}a\lambda + \frac{1}{2}c^2.$$

The characteristic equation of $\mathbf{U_1}$ is expressed as

$$\left(\mu + \frac{a}{2}\right)^2 = \left(\lambda + \frac{a}{2}\right)^2 - c^2. \tag{A3}$$

To facilitate the analyses, we introduce the following transformations to parametrize the algebraic equation Eq. (A3). Then we have

$$\mu + \frac{a}{2} = ic\sin(z), \quad \lambda + \frac{a}{2} = c\cos(z), \tag{A4}$$

with $z \in (0, \pi)$. In this way, the square root's multivalue problem can be neatly solved. Thus, the eigenvalue $\mu = -\frac{a}{2} + i\sin(z)$. Based on Eqs. (A2)–(A4), we obtain the vector solution of Eq. (A1) at the spectral parameter $\lambda_j = -\frac{a}{2} + \kappa_j$, with $\kappa_j = c\cos z_j$ $(j = 1, \ldots, n)$,

$$\mathbf{\Phi}_j = \begin{bmatrix} e^{i\chi_j} \\ e^{i(\theta+\chi_j)}(\lambda_j - \mu_j)/c \end{bmatrix},$$

with $\chi_j = \mu_j x + (\varepsilon_1\mu_j + \varepsilon_2)t$. Then, the n-dark soliton solutions can be derived by applying the n-fold DT [33]. By conducting complicated simplification, the explicit expressions of the n-dark soliton solution can be given in a compact form:

$$q^{[n]} = c\frac{\det(\mathbf{M}_1)}{\det(\mathbf{M})}e^{i\theta}, \tag{A5}$$

where

$$\mathbf{M} = \left(\frac{e^{i(\chi_j - \bar{\chi}_m)} + \delta_{[m,j]}}{e^{iz_j} - e^{-iz_m}}\right)_{1\leqslant m,j\leqslant n},$$

$$\mathbf{M}_1 = \left(\frac{e^{i(\chi_j + z_j - \bar{\chi}_m + z_m)} + \delta_{[m,j]}}{e^{iz_j} - e^{-iz_m}}\right)_{1\leqslant m,j\leqslant n},$$

$$\chi_j = i\sqrt{c^2 - \kappa_1^2}(x - v_j t),$$

$$\delta_{[m,j]} = \begin{cases} 0, & m \neq j \\ e^{2\sqrt{c^2-\kappa_m^2}\gamma_m}, & m = j \end{cases}, \quad j = 1, 2, \ldots, n.$$

$v_j = v_{\mathrm{ds}_j} + a$ is the sum of the soliton velocity and the background velocity. The background velocity equals the value of the wave number based on the quantum mechanics theory [34]. The soliton velocity is given by

$$v_{\mathrm{ds}_j} = \beta\left[4\kappa_j^2 - 6a\kappa_j + 3a^2 + 2c^2\right] - \kappa_j. \tag{A6}$$

The detailed calculations show that the velocity ranges of SVDS have been classified into four cases with the fixing of the sign of high-order nonlinearity coefficient β. The results have been summarized in Table I.

With choosing $n = 1$, Eq. (A5) is the well-known SVDS solution, which can be simplified as Eq. (2). It is seen that the soliton velocity v_{ds_j} is a quadratic function of κ_j, which means that two SVDSs can admit the identical velocity by choosing two different spectral parameters for $q^{[2]}$, which cannot be realized in NLSE. This provides the possibility to construct the two parallel SVDSs mathematically. When the two valleys of these SVDSs are overlapped, the two parallel SVDSs become DVDS. In the following, we intend to derive the DVDS solutions.

The first step and the most critical step in constructing DVDS solutions is to make the velocities of two SVDSs equal, namely, $v_{\mathrm{ds}_1} = v_{\mathrm{ds}_2}$ for the solution $q^{[2]}$. To this end, the following constraint condition should be satisfied:

$$\cos(z_2) = -\cos(z_1) + \rho, \tag{A7}$$

with $\rho = (6a\beta + 1)/(4c\beta)$. Since $-1 < \cos(z_2) < 1$, the following conditions must be satisfied when choosing z_1 related to spectral parameter λ_1:

$$\begin{cases} z_1 \in (0, \arccos[\rho - 1]), & \rho \geqslant 0 \\ z_1 \in (\arccos[\rho + 1], \pi), & \rho < 0 \end{cases}, \tag{A8}$$

When all parameters meet the constraint conditions Eqs. (A7) and (A8), we can obtain two parallel SVDSs.

The second step to forming DVDS is to make two valleys of two parallel SVDSs overlap. In other words, the distance

between two valleys cannot be considerable. Otherwise, the expression $q^{[2]}$ is still the two SVDSs solutions rather than a DVDS solution. This can be realized by adjusting the two free parameters γ_1 and γ_2. Then, we can obtain the DVDS solution based on the two SVDSs solutions $q^{[2]}$. The explicit solution expression of DVDS has been simplified as Eq. (8). The examples for the intensity profiles of DVDS have been shown in Fig. 3.

APPENDIX B: ASYMPTOTIC ANALYSIS

We investigate collision behavior of n-dark solitons which involves n_1 SVDSs and n_2 DVDSs ($n = n_1 + 2n_2$) systematically by developing the asymptotic analysis technique. The n-dark solitons are ranked by velocities, supposing $v_1 \leqslant \cdots \leqslant v_k \leqslant \cdots \leqslant v_n$ ($k = 1, \ldots, n$). Then we will derive the asymptotic expressions q_{s_i} for the ith soliton ($i = 1, \ldots, n_1 + n_2$), which can be an SVDS or a DVDS.

Case 1: When q_{s_i} is an SVDS, which is related to the spectral parameter $\lambda_k = -\frac{a}{2} + c\cos(z_k)$. Its propagation direction is controlled by the function $x - v_k t = \text{const}$, which is contained in the exponential terms $e^{i(\chi_j - \bar{\chi}_j)}$ in the n-dark soliton solution Eq. (A5). Before the collision ($t \to -\infty$), there are $e^{i(\chi_j - \bar{\chi}_j)} \to +\infty$ with $1 \leqslant j < k$ and $e^{i(\chi_j - \bar{\chi}_j)} \to 0$ with $k < j \leqslant n$. To get the asymptotic expressions of q_{s_i} before the collision, we need to further eliminate the terms in which $e^{i(\chi_j - \bar{\chi}_j)} \to \infty$. To this end, $e^{i(\chi_j - \bar{\chi}_j)}$ divide the jth rows of matrices $\mathbf{M_1}$ and $\mathbf{M}$ ($j = 1, \ldots, k-1$) when $t \to -\infty$. Then, the solution Eq. (A5) can be rewritten as

$$q^{[n]} = c\frac{\det(\hat{\mathbf{M}}_\mathbf{1})}{\det(\hat{\mathbf{M}})}e^{i\theta}, \tag{B1}$$

where

$$\hat{\mathbf{M}} = [\hat{\mathbf{M}}^{(1)}, \hat{\mathbf{M}}^{(2)}, \hat{\mathbf{M}}^{(3)}]^\intercal,$$

with

$$\hat{\mathbf{M}}^{(1)} = \left(\frac{e^{i(\chi_j - \chi_i)}}{e^{iz_j} - e^{-iz_i}}\right)_{1\leqslant i\leqslant k-1, 1\leqslant j\leqslant n},$$

$$\hat{\mathbf{M}}^{(2)} = \left(\frac{e^{i(\chi_j - \bar{\chi}_k)} + \delta_{[k,j]}}{e^{iz_j} - e^{-iz_k}}\right)_{1\leqslant j\leqslant n},$$

$$\hat{\mathbf{M}} = \left(\hat{m}^{(i,j)}\right)_{k+1\leqslant i\leqslant n, 1\leqslant j\leqslant n},$$

$$\hat{m}^{(i,j)} = \begin{cases} \frac{\delta_i}{e^{iz_i} - e^{-iz_i}}, & i = j \\ \frac{e^{i(\chi_j - \bar{\chi}_i)}}{e^{iz_j} - e^{-iz_i}}, & i \neq j \end{cases}.$$

Here, we define $\delta_{[i,i]}$ as δ_i. Similarly,

$$\hat{\mathbf{M}}_\mathbf{1} = \left[\hat{\mathbf{M}}_\mathbf{1}^{(1)}, \hat{\mathbf{M}}_\mathbf{1}^{(2)}, \hat{\mathbf{M}}_\mathbf{1}^{(3)}\right]^\intercal,$$

where

$$\hat{\mathbf{M}}_\mathbf{1}^{(1)} = \left(\frac{e^{i(X_j - z_j - X_i - z_i)}}{e^{iz_j} - e^{-iz_i}}\right)_{1\leqslant i\leqslant k-1, 1\leqslant j\leqslant n},$$

$$\hat{\mathbf{M}}_\mathbf{1}^{(2)} = \left(\frac{e^{i(X_j - z_j - \bar{X}_k - z_k)} + \delta_{[k,j]}}{e^{iz_j} - e^{-iz_i}}\right)_{1\leqslant j\leqslant n},$$

$$\hat{\mathbf{M}}_\mathbf{1}^{(3)} = \left(\hat{m}_1^{(i,j)}\right)_{k+1\leqslant i\leqslant n, 1\leqslant j\leqslant n},$$

$$\hat{m}_1^{(i,j)} = \begin{cases} \frac{\delta_i}{e^{iz_i} - e^{-iz_i}}, & i = j \\ \frac{e^{i(X_j - z_j - \bar{X}_i - z_i)}}{e^{iz_j} - e^{-iz_i}}, & i \neq j \end{cases}.$$

By direct calculation, we have

$$\det(\hat{\mathbf{M}}) = \prod_{i=k+1}^{n}\frac{\delta_i}{e^{iz_i} - e^{-iz_i}}\left[e^{i(\chi_k - \bar{\chi}_k)}\det(\mathbf{F}_k) + \frac{\delta_k}{e^{iz_k} - e^{-iz_k}}\det(\mathbf{F}_{k-1})\right],$$

where

$$\mathbf{F}_l = \left(\frac{1}{e^{iz_j} - e^{-iz_i}}\right)_{l\leqslant i,j\leqslant l}, \quad l = k-1, k.$$

Obviously, $\mathbf{F}_l$ is a Cauchy matrix, thus

$$\det(\mathbf{F}_l) = \frac{\prod_{j=2}^{l}\prod_{i=1}^{j-1}(e^{iz_j} - e^{iz_i})(e^{-iz_i} - e^{-iz_j})}{\prod_{j=1}^{l}\prod_{i=1}^{l}(e^{iz_i} - e^{-iz_j})}.$$

Similarly,

$$\det(\hat{\mathbf{M}}_1) = \prod_{i=k+1}^{n}\frac{\delta_i}{e^{iz_i} - e^{-iz_i}}\left[e^{i(\chi_k - \bar{\chi}_k)}\det(\mathbf{G}_k) + \frac{\delta_k}{e^{iz_k} - e^{-iz_k}}\det(\mathbf{G}_{k-1})\right],$$

with $\det(\mathbf{G}_l) = \prod_{i=1}^{l} e^{-2iz_i}\det(\mathbf{F}_l)$. Thus, when $t \to -\infty$ the asymptotic behavior of SVDS can be derived as

$$q_{s_i}^- = cL_{s_i}^-[1 - B_k + B_k\tanh(Y_{s_i}^-)]e^{i\theta}, \tag{B2}$$

where

$$B_k = i\sin(z_k)\,e^{-iz_k},$$

$$L_{s_i}^- = \prod_{m=1}^{k-1} e^{-2iz_m}, \quad K_1^- = \prod_{i=1}^{k-1}\omega_{[k,i]},$$

$$Y_{s_i}^- = c\sin(z_k)(x - v_k t + \gamma_k) - \ln|K_1^-|.$$

When $t \to +\infty$, we can also derive the asymptotic solution of SVDS in a similar way,

$$q_{s_i}^+ = cL_{s_i}^+[1 - B_k + B_k\tanh(Y_{s_i}^+)]e^{i\theta}, \tag{B3}$$

where

$$L_{s_i}^+ = \prod_{m=k+1}^{n} e^{-2iz_m}, \quad K_1^+ = \prod_{i=k+1}^{n}\omega_{[k,i]},$$

$$Y_{s_i}^+ = c\sin(z_k)(x - v_k t + \gamma_k) - \ln|K_1^+|,$$

and $\omega_{[k,i]} = \frac{\sin(\frac{z_k - z_i}{2})}{\sin(\frac{z_k + z_i}{2})}$.

Case 2: When q_{s_i} is a DVDS, which is related to the spectral parameters $\lambda_k = -\frac{a}{2} + c\cos(z_k)$ and $\lambda_{k+1} = -\frac{a}{2} + c\cos(z_{k+1})$. Then we analyze the asymptotic behavior of DVDS before and after the collision along the propagating direction $x - v_k t = x - v_{k+1} t = \text{const}$. Before the collision ($t \to -\infty$), there are $e^{i(\chi_j - \bar{\chi}_j)} \to +\infty$ for $j < k$, and $e^{i(\chi_j - \bar{\chi}_j)} \to 0$ for $j > k+1$. Then, $e^{i(\chi_j - \bar{\chi}_j)}$ divide the

jth rows of both matrices $\mathbf{M_1}$ and $\mathbf{M}$ ($j = 1, \ldots, k-1$) and taking the limit $t \to -\infty$, then the solution Eq. (A5) can be rewritten as

$$q^{[n]} = c\frac{\det(\hat{\mathbf{M}}_\mathbf{1})}{\det(\hat{\mathbf{M}})}e^{i\theta}, \tag{B4}$$

where

$$\hat{\mathbf{M}} = [\hat{\mathbf{M}}^{(1)}, \hat{\mathbf{M}}^{(2)}, \hat{\mathbf{M}}^{(3)}]^\intercal,$$

with

$$\hat{\mathbf{M}}^{(1)} = \left(\frac{e^{i(\chi_j-\chi_i)}}{e^{iz_j}-e^{-iz_i}}\right)_{1\leqslant i\leqslant k-1, 1\leqslant j\leqslant n},$$
$$\hat{\mathbf{M}}^{(2)} = \left(\frac{e^{i(\chi_j-\bar{\chi}_i)}+\delta_{[i,j]}}{e^{iz_j}-e^{-iz_i}}\right)_{k\leqslant i\leqslant k+1, 1\leqslant j\leqslant n},$$
$$\hat{\mathbf{M}}^{(3)} = (\hat{m}^{(i,j)})_{k+2\leqslant i\leqslant n, 1\leqslant j\leqslant n},$$
$$\hat{m}^{(i,j)} = \begin{cases} \frac{\delta_i}{e^{iz_i}-e^{-iz_i}}, & i=j \\ \frac{e^{i(\chi_j-\bar{\chi}_i)}}{e^{iz_j}-e^{-iz_i}}, & i\neq j \end{cases}.$$

We can also write $\hat{\mathbf{M}}_\mathbf{1}$ as

$$\hat{\mathbf{M}}_\mathbf{1} = \left[\hat{\mathbf{M}}_\mathbf{1}^{(1)}, \hat{\mathbf{M}}_\mathbf{1}^{(2)}, \hat{\mathbf{M}}_\mathbf{1}^{(3)}\right]^\intercal,$$

with

$$\hat{\mathbf{M}}_\mathbf{1}^{(1)} = \left(\frac{e^{i(\chi_j-z_j-\chi_i-z_i)}}{e^{iz_j}-e^{-iz_i}}\right)_{1\leqslant i\leqslant k-1, 1\leqslant j\leqslant n},$$
$$\hat{\mathbf{M}}_\mathbf{1}^{(2)} = \left(\frac{e^{i(\chi_j-z_j-\bar{\chi}_i-z_i)}+\delta_{[i,j]}}{e^{iz_j}-e^{-iz_i}}\right)_{k\leqslant i\leqslant k+1, 1\leqslant j\leqslant n},$$
$$\hat{\mathbf{M}}_\mathbf{1}^{(3)} = \left(\hat{m}_1^{(i,j)}\right)_{k+2\leqslant i\leqslant n, 1\leqslant j\leqslant n},$$
$$\hat{m}_1^{(i,j)} = \begin{cases} \frac{\delta_i}{e^{iz_i}-e^{-iz_i}}, & i=j \\ \frac{e^{i(\chi_j-z_j-\bar{\chi}_i-z_i)}}{e^{iz_j}-e^{-iz_i}}, & i\neq j \end{cases}.$$

Then the determinant of $\hat{\mathbf{M}}$ and $\hat{\mathbf{M}}_\mathbf{1}$ can be written as

$$\begin{aligned}
&\det(\hat{\mathbf{M}}) \\
&= \prod_{i=k+2}^{n}\frac{\delta_i}{e^{iz_i}-e^{-iz_i}}\Bigg[e^{i[(\chi_k-\bar{\chi}_k)+(\chi_{k+1}-\bar{\chi}_{k+1})]}\det(\mathbf{F}_{k+1}) \\
&\quad + \frac{\delta_k e^{i(\chi_{k+1}-\bar{\chi}_{k+1})}}{e^{iz_k}-e^{-iz_k}}\det(\hat{\mathbf{F}}_k) + \frac{\delta_{k+1}e^{i(\chi_k-\bar{\chi}_k)}}{e^{iz_{k+1}}-e^{-iz_{k+1}}}\det(\mathbf{F}_k) \\
&\quad + \frac{\delta_k\delta_{k+1}}{(e^{iz_k}-e^{-iz_k})(e^{iz_{k+1}}-e^{-iz_{k+1}})}\det(\mathbf{F}_{k-1})\Bigg], \\
&\det(\hat{\mathbf{M}}_\mathbf{1}) \\
&= \prod_{i=k+2}^{n}\frac{\delta_i}{e^{iz_i}-e^{-iz_i}}\Bigg[e^{i[(\chi_k-\bar{\chi}_k)+(\chi_{k+1}-\bar{\chi}_{k+1})]}\det(\mathbf{G}_{k+1}) \\
&\quad + \frac{\delta_k e^{i(\chi_{k+1}-\bar{\chi}_{k+1})}}{e^{iz_k}-e^{-iz_k}}\det(\hat{\mathbf{G}}_k) + \frac{\delta_{k+1}e^{i(\chi_k-\bar{\chi}_k)}}{e^{iz_{k+1}}-e^{-iz_{k+1}}}\det(\mathbf{G}_k) \\
&\quad + \frac{\delta_k\delta_{k+1}}{(e^{iz_k}-e^{-iz_k})(e^{iz_{k+1}}-e^{-iz_{k+1}})}\det(\mathbf{G}_{k-1})\Bigg],
\end{aligned}$$

where

$$\det(\mathbf{F}_l) = \frac{\prod_{j=2}^{l}\prod_{i=1}^{j-1}(e^{iz_j}-e^{iz_i})(e^{-iz_i}-e^{-iz_j})}{\prod_{j=1}^{l}\prod_{i=1}^{l}(e^{iz_i}-e^{-iz_j})},$$
$$\det(\hat{\mathbf{F}}_k) = \prod_{i=1}^{k-1}\frac{(e^{iz_{k+1}}-e^{iz_i})(e^{-iz_i}-e^{-iz_{k+1}})}{(e^{iz_{k+1}}-e^{-iz_i})(e^{iz_i}-e^{-iz_{k+1}})} \times \frac{1}{e^{iz_{k+1}}-e^{-iz_{k+1}}}\det(\mathbf{F}_{k-1}),$$
$$\det(\mathbf{G}_l) = \prod_{i=1}^{l}e^{-2iz_i}\det(\mathbf{F}_l), \quad l = k-1, k, k+1,$$
$$\det(\hat{\mathbf{G}}_k) = \prod_{i=1}^{k-1}e^{-2iz_i}e^{-2iz_{k+1}}\det(\hat{\mathbf{F}}_k).$$

Thus, the asymptotic behavior of the DVDS at $t \to -\infty$ is expressed as

$$q_{s_i}^- = c\frac{\det(\hat{\mathbf{M}}_1)}{\det(\hat{\mathbf{M}})}e^{i\theta} = cL_{s_i}^-\frac{N_{s_i}^-}{D_{s_i}^-}e^{i\theta}. \tag{B5}$$

By performing the similar procedure as presented above, along the trajectory $x - v_k t = x - v_{k+1}t = \text{const}$ at $t \to +\infty$, we get the asymptotic expression of DVDS after the collision as the following form:

$$q_{s_i}^+ = c\frac{\det(\hat{\mathbf{M}}_1)}{\det(\hat{\mathbf{M}})}e^{i\theta} = cL_{s_i}^+\frac{N_{s_i}^+}{D_{s_i}^+}e^{i\theta}, \tag{B6}$$

where

$$\begin{aligned}
N_{s_i}^\pm &= K_2^\pm e^{-\eta_k-\eta_{k+1}} + K_3^\pm e^{\eta_k-\eta_{k+1}} + K_4^\pm e^{\eta_{k+1}-\eta_k} \\
&\quad + e^{\eta_k+\eta_{k+1}}, \\
D_{s_i}^\pm &= K_2^\pm e^{-\xi_k-\xi_{k+1}} + K_3^\pm e^{\xi_k-\xi_{k+1}} + K_4^\pm e^{\xi_{k+1}-\xi_k} \\
&\quad + e^{\xi_k+\xi_{k+1}},
\end{aligned}$$

and

$$L_{s_i}^- = \prod_{m=1}^{k-1}e^{-2iz_m}, \qquad L_{s_i}^+ = \prod_{m=k+2}^{n}e^{-2iz_m},$$
$$K_2^- = \prod_{j=k}^{k+1}\prod_{i=1}^{j-1}\omega_{[j,i]}^2, \qquad K_2^+ = \prod_{j=k}^{k+1}\prod_{i=j+1}^{n}\omega_{[j,i]}^2,$$
$$K_3^- = \prod_{i=1}^{k-1}\omega_{[k+1,i]}^2, \qquad K_3^+ = \prod_{i=k+2}^{n}\omega_{[k+1,i]}^2,$$
$$K_4^- = \prod_{i=1}^{k-1}\omega_{[k,i]}^2, \qquad K_4^+ = \prod_{i=k+2}^{n}\omega_{[k,i]}^2.$$

In addition, we let $\prod_{m=1}^{k-1} f = 1$ when $k = 1$, and $\prod_{m=k+1}^{n} f = 1$ when $k = n$, where $f = \omega^2$ or e^{-2iz_m} in above related expressions.

APPENDIX C: THE ELASTIC COLLISION FOR SVDS AND DVDS

The asymptotic results Eqs. (B2), (B3), (B5), and (B6) provide the fundamental conditions to analyze their collision properties directly and exactly. From Eqs. (B2) and (B3), we can easily get

$$|q_{s_i}^-(x+x_1)|^2 = |q_{s_i}^+(x+x_2)|^2,$$

with

$$x_1 = \frac{\ln|K_1^-|}{c\sin(z_k)}, \quad x_2 = \frac{\ln|K_1^+|}{c\sin(z_k)}.$$

This demonstrates that SVDS survives its shape after the collision with a phase shift, similar to the solitons' collision reported before. However, DVDS does not admit such property in the general case, as shown in Fig. 5. Then we would like to know whether the collision of DVDS can also be elastic. We rewrite Eqs. (B5) and (B6) in the following form to facilitate our analyses:

$$|q_{s_i}^\pm|^2 = c^2[1+\partial_{xx}\ln(D_{s_i}^\pm)]. \tag{C1}$$

When the collision of n-dark solitons is elastic for the DVDS q_{s_i} which is related to the spectral parameters λ_k and λ_{k+1}, it will only result in a phase shift. Thus, we can assume $|q_{s_i}^-(x+c_1)|^2 = |q_{s_i}^+(x)|^2$, where c_1 is a constant. According to Eq. (C1), we just need to let $D_{s_i}^-(x+c_1) = D_{s_i}^+(x)$. Then, we have

$$\begin{aligned}\ln(K_3^+) &= \ln(K_3^-) - c\sin(z_{k+1})c_1,\\ \ln(K_4^+) &= \ln(K_4^-) - c\sin(z_k)c_1.\end{aligned} \tag{C2}$$

Based on Eq. (C2), we get

$$\frac{\ln(K_3^+)-\ln(K_3^-)}{\ln(K_4^+)-\ln(K_4^-)} = \frac{\sin(z_{k+1})}{\sin(z_k)}. \tag{C3}$$

Therefore, under this condition, the collisions contained DVDSs can be elastic. In other words, this is the sufficient condition, Eq. (C3), of elastic interaction for DVDSs.

[1] L. F. Mollenauer, R. H. Stolen, and J. P. Gordon, Experimental Observation of Picosecond Pulse Narrowing and Solitons in Optical Fibers, Phys. Rev. Lett. **45**, 1095 (1980).

[2] A. M. Weiner, J. P. Heritage, R. J. Hawkins, R. N. Thurston, E. M. Kirschner, D. E. Leaird, and W. J. Tomlinson, Experimental Observation of the Fundamental Dark Soliton in Optical Fibers, Phys. Rev. Lett. **61**, 2445 (1988).

[3] Y. S. Kivshar and G. P. Agrawal, *Optical Solitons: From Fibers to Photonic Crystals* (Academic Press, New York, 2003).

[4] Y. S. Kivshar and B. Luther-Davies, Dark optical solitons: Physics and applications, Phys. Rep. **298**, 81 (1998).

[5] Y. Song, X. Shi, C. Wu, D. Tang, and H. Zhang, Recent progress of study on optical solitons in fiber lasers, Appl. Phys. Rev. **6**, 021313 (2019).

[6] A. Hasegawa and F. Tappert, Transmission of stationary nonlinear optical pulses in dispersive dielectric fibers. II. Normal dispersion, Appl. Phys. Lett. **23**, 171 (1973).

[7] A. Hasegawa and F. Tappert, Transmission of stationary nonlinear optical pulses in dispersive dielectric fibers. I. Anomalous dispersion, Appl. Phys. Lett. **23**, 142 (1973).

[8] D. J. Frantzeskakis, Dark solitons in atomic Bose-Einstein condensates: From theory to experiments, J. Phys. A: Math. Theor. **43**, 213001 (2010).

[9] J. R. Anglin, Local Vortex Generation and the Surface Mode Spectrum of Large Bose-Einstein Condensates, Phys. Rev. Lett. **87**, 240401 (2001).

[10] S. Donadello, S. Serafini, M. Tylutki, L. P. Pitaevskii, F. Dalfovo, G. Lamporesi, and G. Ferrari, Observation of Solitonic Vortices in Bose-Einstein Condensates, Phys. Rev. Lett. **113**, 065302 (2014).

[11] I. V. Barashenkov and E. Y. Panova, Stability and evolution of the quiescent and travelling solitonic bubbles, Physica D **69**, 114 (1993).

[12] I. V. Barashenkov, Stability Criterion for Dark Solitons, Phys. Rev. Lett. **77**, 1193 (1996).

[13] L.-C. Zhao, Y.-H. Qin, C. Lee, and J. Liu, Classification of dark solitons via topological vector potentials, Phys. Rev. E **103**, L040204 (2021).

[14] Y.-H. Qin, L.-C. Zhao, Z.-Q. Yang, and L.-M. Ling, Multivalley dark solitons in multicomponent Bose-Einstein condensates with repulsive interactions, Phys. Rev. E **104**, 014201 (2021).

[15] K. Porsezian, Soliton propagation in nonlinear optics with higher-order effects, J. Mod. Opt. **44**, 387 (1997).

[16] A. Mahalingam and K. Porsezian, Propagation of dark solitons with higher-order effects in optical fibers, Phys. Rev. E **64**, 046608 (2001).

[17] R. Hirota, Exact envelope-soliton solutions of a nonlinear wave equation, J. Math. Phys. **14**, 805 (1973).

[18] Y. Kodama and A. Hasegawa, Nonlinear pulse propagation in a monomode dielectric guide, IEEE J. Quantum Electron. **23**, 510 (1987).

[19] K. Porsezian and K. Nakkeeran, Optical Solitons in Presence of Kerr Dispersion and Self-Frequency Shift, Phys. Rev. Lett. **76**, 3955 (1996).

[20] L. Li, Z. Li, Z. Xu, G. Zhou, and K. H. Spatschek, Gray optical dips in the subpicosecond regime, Phys. Rev. E **66**, 046616 (2002).

[21] C. Wu, B. Wei, C. Shi, and B.-F. Feng, Multi-breather solutions to the Sasa-Satsuma equation, Proc. R. Soc. A **478**, 20210711 (2022).

[22] B.-F. Feng, C. Shi, G. Zhang, and C. Wu, Higher-order rogue wave solutions of the Sasa-Satsuma equation, J. Phys. A: Math. Theor. **55**, 235701 (2022).

[23] X.-M. Zhang, Y.-H. Qin, L.-M. Ling, and L.-C. Zhao, Inelastic interaction of double-valley dark solitons for the Hirota equation, Chin. Phys. Lett. **38**, 090201 (2021).

[24] D.-H. Xu and S.-Y. Lou, Dark soliton molecules in nonlinear optics, Acta Phys. Sin. **69**, 014208 (2020).

[25] S. M. Hoseini and T. R. Marchant, Evolution of higher-order gray Hirota solitary waves, Stud. Appl. Math. **121**, 117 (2008).
[26] H.-Q. Zhang and S.-S. Yuan, Dark soliton solutions of the defocusing Hirota equation by the binary Darboux transformation, Nonlin. Dyn. **89**, 531 (2017).
[27] D. Mihalache, N. Truta, and L.-C. Crasovan, Painlevé analysis and bright solitary waves of the higher-order nonlinear Schrödinger equation containing third-order dispersion and self-steepening term, Phys. Rev. E **56**, 1064 (1997).
[28] A. Ankiewicz, J. M. Soto-Crespo, and N. Akhmediev, Rogue waves and rational solutions of the Hirota equation, Phys. Rev. E **81**, 046602 (2010).
[29] Y. Tao and J. He, Multisolitons, breathers, and rogue waves for the Hirota equation generated by the Darboux transformation, Phys. Rev. E **85**, 026601 (2012).
[30] A. Chowdury, A. Ankiewicz, and N. Akhmediev, Moving breathers and breather-to-soliton conversions for the Hirota equation, Proc. R. Soc. A **471**, 20150130 (2015).
[31] X.-E. Zhang and L.-M. Ling, Asymptotic analysis of high-order solitons for the Hirota equation, Physica D **426**, 132982 (2021).
[32] S. Chen and L. Y. Song, Rogue waves in coupled Hirota systems, Phys. Rev. E **87**, 032910 (2013).
[33] L. Ling, L.-C. Zhao, and B. Guo, Darboux transformation and multi-dark soliton for N-component nonlinear Schrödinger equations, Nonlinearity **28**, 3243 (2015).
[34] L. D. Landau and E. M. Lifshits, *Quantum Mechanics* (Nauka, Moscow, 1989).
[35] R. Radhakrishnan and M. Lakshmanan, Exact soliton solutions to coupled nonlinear Schrödinger equations with higher-order effects, Phys. Rev. E **54**, 2949 (1996).
[36] C. Liu, Z.-Y. Yang, L.-C. Zhao, L. Duan, G. Yang, and W.-L. Yang, Symmetric and asymmetric optical multipeak solitons on a continuous wave background in the femtosecond regime, Phys. Rev. E **94**, 042221 (2016).
[37] Y.-H. Wu, L.-C. Zhao, C. Liu, Z.-Y. Yang, and W.-L. Yang, The topological phase of bright solitons, Phys. Lett. A **434**, 128045 (2022).
[38] L.-C. Zhao, L.-Z. Meng, Y.-H. Qin, Z.-Y. Yang, and J. Liu, Topological vector potentials underlying one-dimensional nonlinear waves, arXiv:2102.10914v1.
[39] W. K. Hayman, *Meromorphic Functions* (Oxford University Press, Oxford, UK, 1964).
[40] J. Wess and B. Zumino, Consequences of anomalous ward identities, Phys. Lett. B **37**, 95 (1971).
[41] D. Xiao, M.-C. Chang, and Q. Niu, Berry phase effects on electronic properties, Rev. Mod. Phys. **82**, 1959 (2010).
[42] M. V. Berry, Quantal phase factors accompanying adiabatic changes, Proc. R. Soc. London A **392**, 45 (1984).
[43] D. W. Aossey, S. R. Skinner, J. L. Cooney, and J. E. Williams, Properties of soliton-soliton collisions, Phys. Rev. A **45**, 2606 (1992).
[44] G. Huang and M. G. Velarde, Head-on collisions of dark solitons near the zero-dispersion point in optical fibers, Phys. Rev. E **54**, 3048 (1996).
[45] J. H. V. Nguyen, P. Dyke, D. Luo, B. A. Malomed, and R. G. Hulet, Collisions of matter-wave solitons, Nat. Phys. **10**, 918 (2014).
[46] C. Liu, Z.-Y. Yang, L.-C. Zhao, and W.-L. Yang, Vector breathers and the inelastic interaction in a three-mode nonlinear optical fiber, Phys. Rev. A **89**, 055803 (2014).
[47] L.-C. Zhao, L. Ling, Z.-Y. Yang, and J. Liu, Properties of the temporal-spatial interference pattern during soliton interaction, Nonlinear Dyn. **83**, 659 (2016).
[48] S. Stalin, R. Ramakrishnan, M. Senthilvelan, and M. Lakshmanan, Nondegenerate Solitons in Manakov System, Phys. Rev. Lett. **122**, 043901 (2019).
[49] Y.-H. Qin, L.-C. Zhao, and L. Ling, Nondegenerate bound-state solitons in multicomponent Bose-Einstein condensates, Phys. Rev. E **100**, 022212 (2019).
[50] R. Ramakrishnan, S. Stalin, and M. Lakshmanan, Nondegenerate solitons and their collisions in Manakov system, Phys. Rev. E **102**, 042212 (2020).
[51] Y.-H. Qin, Y. Wu, L.-C. Zhao, and Z.-Y. Yang, Interference properties of two-component matter wave solitons, Chin. Phys. B **29**, 020303 (2020).